Self-Assembly

Deutsche Ausgabe: DOI: 10.1002/ange.201605696
Internationale Ausgabe: DOI: 10.1002/anie.201605696

Reciprocal Self-Assembly of Peptide–DNA Conjugates into a Programmable Sub-10-nm Supramolecular Deoxyribonucleoprotein

*Mahnseok Kye and Yong-beom Lim**

Abstract: *To overcome the limitations of molecular assemblies, the development of novel supramolecular building blocks and self-assembly modes is essential to create more sophisticated, complex, and controllable aggregates. The self-assembly of peptide–DNA conjugates (PDCs), in which two orthogonal self-assembly modes, that is, β-sheet formation and Watson–Crick base pairing, are covalently combined in one supramolecular system, is reported. Despite extensive research, most self-assembly studies have focused on using only one type of building block, which restricts structural and functional diversity compared to multicomponent systems. Multicomponent systems, however, suffer from poor control of self-assembly behaviors. Covalently conjugated PDC building blocks are shown to assemble into well-defined and controllable nanostructures. This controllability likely results from the decrease in entropy associated with the restriction of the molecular degrees of freedom by the covalent constraints. Using this strategy, the possibility to thermodynamically program nano-assemblies to exert gene regulation activity with low cytotoxicity is demonstrated.*

Although many different types of supramolecular building blocks and assembly strategies have been devised,[1] human control of the self-assembly process is still far behind that of nature. Biopolymers such as peptides[2] and nucleic acids (DNAs and RNAs)[3] are important supramolecular building blocks for nanotechnology. Most bottom-up nanostructures assembled from these biopolymers have been constructed utilizing only one type of building block. However, in biological systems, there are many examples of functional supramolecular complexes composed of multiple proteins and nucleic acids, known as nucleoproteins. For example, viruses can be viewed as supramolecular complexes of DNA/protein (deoxyribonucleoproteins; DNPs) or RNA/protein (ribonucleoproteins; RNPs), depending on their genome type. Other important examples of nucleoproteins include nucleosomes, ribosomes, telomerase, heterogeneous nuclear ribonucleoproteins (hnRNPs), and small nuclear RNPs (snRNPs).

The fundamentally different properties of nucleic acids and proteins can potentially provide synergistic effects when combined properly. Thus, combining these two biopolymers into one supramolecular system may be a strategy for constructing artificial nanostructures with new and superior functions. However, the construction of such structures through supramolecular approaches has proven challenging because of the difficulty of controlling the self-assembly process. For example, a DNA/polymer complex for gene delivery, that is, an artificial virus, is one of the most widely used examples of a synthetic nucleic acid/biopolymer complex.[4] Although some success has been achieved in forming relatively well-defined artificial viruses[5] and molecular assemblies of DNA–polymer conjugates,[6] supramolecular complexes of polymer and DNA have mostly resulted in the formation of heterogeneous particles. In contrast, nature has developed a precisely controllable DNA packaging mechanism, nucleosome formation, by utilizing histone proteins.[7] Although nature uses a totally noncovalent strategy, human control of the self-assembly process is still too immature to construct discrete multicomponent supramolecular assemblies solely using noncovalent interactions.

Herein, we report the development of a well-defined supramolecular DNP through self-assembly of peptide–DNA conjugates (PDCs), in which the disparate assembly modes of DNA and peptides are exquisitely combined into one supramolecular nanostructure (Figure 1). We hypothesized that the use of covalently conjugated peptides and DNA would reduce the number of degrees of freedom that the supramolecular building blocks need to sample, thus simplifying the overall assembly process and increasing the probability of fabricating well-defined nanocomplexes. In this report, the peptide and DNA used β-sheet formation and Watson–Crick base pairing as modes of interaction, respectively.

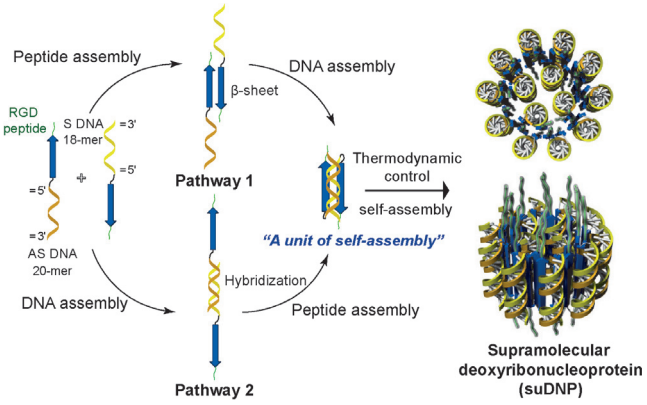

Figure 1. Pathways for the dual-mode self-assembly of complementary peptide–DNA conjugates into a toroidal global minimum state.

[*] M. Kye, Prof. Y.-b. Lim
Department of Materials Science and Engineering, Yonsei University
50 Yonsei-ro, Seoul, 03722 (Korea)
E-mail: yblim@yonsei.ac.kr

Supporting information and the ORCID identification number(s) for the author(s) of this article can be found under http://dx.doi.org/10.1002/anie.201605696.

The synthesis of self-assembling PDCs can be complicated by the aggregation propensity of the peptide segment. We therefore used a solid-phase fragment condensation method that combines the advantages of in-line synthesis and fragment conjugation methods.[8] In-line synthesis methods, in which the peptide and DNA chains are assembled on a resin by stepwise coupling reactions, are often limited by the incompatibility of the deprotection chemistry of peptides and DNA.[8a,b] The fragment conjugation method utilizes the deprotected peptide and DNA, and the conjugation reaction is typically performed in an aqueous solution, a good solvent for both peptides and DNA. Owing to the aggregation propensity of self-assembling peptides, this method can elicit solubility problems. The solid-phase fragment condensation method ligates the deprotected peptide, while the protected DNA remains bound to the solid support. An organic solvent that effectively suppresses the aggregation of the peptides can be used to solvate the reactants in on-resin fragment ligation because both the self-assembling peptides and protected DNAs typically have high degrees of nonpolar character. Using this on-resin fragment ligation, we successfully conjugated DNA oligonucleotides to a self-assembling β-sheet peptide (Supporting Information, Figure S1). The self-assembling peptide, **β-suRGD**, contained a β-sheet self-assembly segment and an Arg-Gly-Asp (RGD) segment for cell internalization. The **β-suRGD** peptide was conjugated to a 20-mer antisense (AS) DNA targeted against green fluorescent protein (GFP) and an 18-mer sense (S) DNA to yield **β-suRGD-AS** and **β-suRGD-S**, respectively.

For dual-mode self-assembly of the peptide-DNA conjugates, **β-suRGD-AS** and **β-suRGD-S** were mixed at a 1:1 molar ratio and their self-assembly behavior was examined. Owing to the presence of disparate self-assembly modes, that is, β-sheet interactions and Watson–Crick hybridization, and two different molecules, the assembly pathways and the final state can be complex. We hypothesized two probable scenarios for the formation of the thermodynamically stable supramolecular complex (Figure 1). First, a condition that enables the formation of a peptide β-sheet followed by DNA hybridization was investigated (pathway 1). Equimolar amounts of both conjugates were dissolved in hexafluoroisopropanol (HFIP). HFIP has a strong propensity to induce the formation of α-helices in any peptide.[9] This tendency, combined with the nonpolar characteristics of HFIP, will destabilize the β-sheet self-assembly mode of the **β-suRGD** segment. After prolonged incubation, the HFIP was evaporated and the dried mixture was redissolved in TE buffer. The aqueous mixture was vigorously sonicated, incubated at a temperature above the melting temperature (T_m) of the duplex (see below), and subsequently cooled down slowly to anneal the duplex. Second, the duplex was hybridized first, and then β-sheet formation was induced (pathway 2). An equimolar mixture was dissolved in aqueous solution at a concentration below the critical aggregation concentration (CAC) of the β-sheet peptide. After annealing the duplex at this low concentration, the solution was slowly concentrated using a centrifugal filtration device to induce assembly of the peptide.

Investigation of the assembly status using various techniques revealed that the two pathways resulted in the formation of identical nanostructures with a homogeneous distribution. Thus, both pathways led to the formation of thermodynamically stable **β-suRGD-AS/β-suRGD-S** complexes (supramolecular deoxyribonucleoprotein; **suDNP**). By comparison, simple dissolution of the aqueous mixture resulted in the formation of a heterogeneous population of nanostructures, suggesting the coexistence of kinetically trapped states and a thermodynamically stable state.

The circular dichroism (CD) spectrum of the **suDNP** revealed negative bands at 207 nm and 254 nm and a positive band at 280 nm (Figure 2a), which is a typical characteristic of B-form DNA.[10] The CD spectrum of the duplex revealed a similar spectral pattern (Supporting Information, Figure S5a). Figure 2a also shows a weak shoulder at approximately 215–220 nm, a signature of β-sheet structures. Isolation of the contribution from the peptide, achieved by subtracting the duplex-only spectrum from the spectrum of

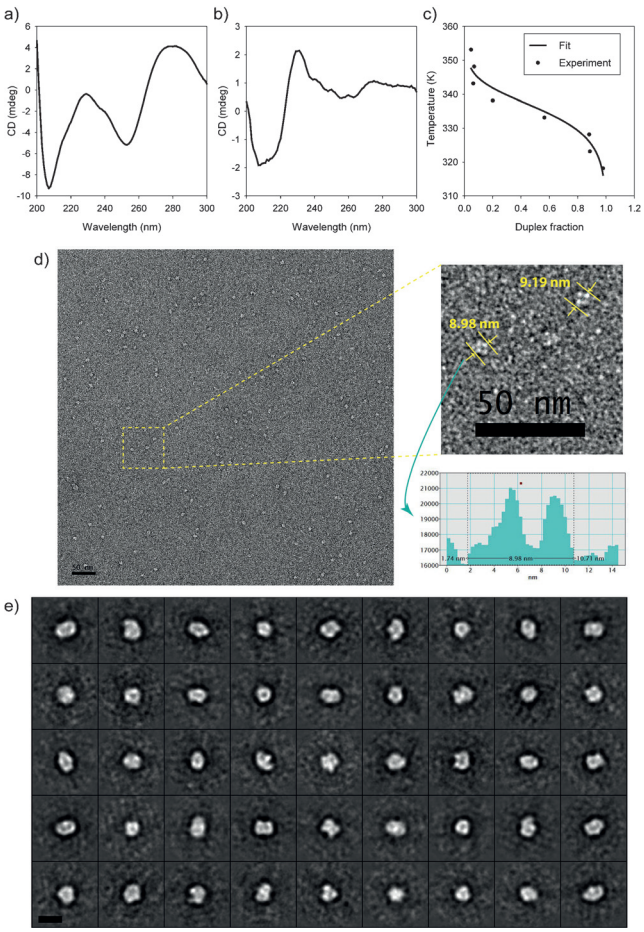

Figure 2. Characterization of the **suDNP**. a) CD spectrum of the **suDNP**. b) CD difference spectrum. c) Melting curve analysis of the **suDNP**. d) An electron micrograph of a negatively stained **suDNP**. Upper right: Enlargement of a region of the electron micrograph. Lower right: line plot display of the **suDNP**. Bar = 50 nm. e) Single particle analysis of TEM images. The 50 representative class average images from 5035 **suDNP** particles from different projection directions. Bar = 10 nm.

the **suDNP**, confirmed β-sheet formation, as indicated by the strong negative band at approximately 217 nm (Figure 2b). This difference spectrum was also similar to that of the peptide only (Supporting Information, Figure S5b). Fourier transform infrared spectroscopy (FTIR) revealed amide I bands at 1633 cm^{-1} and 1695 cm^{-1}, indicating the formation of antiparallel β-sheets (Supporting Information, Figure S6).[11] Thus, the **suDNP** forms through the bipartite assembly mode of double-stranded B-form DNA hybridization and antiparallel β-sheet formation. The cooperative melting transition behavior of the **suDNP** further confirmed the formation of double-stranded DNA (Figure 2c). The melting temperature (T_m) of **suDNP**, 62 °C, was similar to that of the duplex only, 63 °C (Supporting Information, Figure S7). Transmission electron microscopy (TEM) revealed that the size of the **suDNP** particles was approximately 9 nm (Figure 2d). The line plot display of the **suDNP** revealed a concave region in the middle of the **suDNP** in many particle populations. The presence of central pores within the spherical nanostructures was corroborated by 2D reconstruction of electron micrographs to obtain the class average images of single particles and 3D reconstruction (Figure 2e and the Supporting Information, Figure S8). A group of images corresponding to the same projection direction were grouped together and averaged to produce the class average image.[12] Atomic force microscopy (AFM) investigation showed the formation of discrete objects with spherical shapes (Supporting Information, Figure S9). The diameter of the nanostructures measured by AFM was slightly larger than that obtained by TEM, possibly due to the tip-broadening effect.[13] Dynamic light scattering (DLS) further confirmed that particles with approximately 9 nm in diameter exist in solution with a homogeneous size distribution (Supporting Information, Figure S10).

These results allowed us to construct a model for the self-assembled **suDNP** (Figure 1. For a DNA helix diameter of 2 nm and an intersheet distance of 10 Å for bilayered β-sheets (β-sandwiches),[15] the diagonal line across the circular object of circa 9 nm would consist of four DNA helices and one β-sandwich. The presence of the central pore is due to the electrostatic repulsion among the central DNA helices, which results in the formation of toroidal objects. Due to the antiparallel arrangement of the β-sheets, the RGD peptides are located at both faces of the toroid. Although there was a possibility of supramolecular polymerization[16] that would compete with the formation of the toroids, the covalent constraint of the peptide–DNA conjugates effectively suppressed this possibility and enabled the formation of homogeneous toroids.

The **suDNP** was designed such that the AS DNA/mRNA duplex (20-mer/20-mer) is slightly more stable than the AS DNA/S DNA duplex (20-mer/18-mer) owing to differences in their free energy (ΔG) values of hybridization (Figure 3a). We anticipated that the 18-mer S DNA segment in the **suDNP** would be exchanged in the presence of mRNA containing a 20-mer sequence complementary to the AS DNA, thus leading to the inhibition of translation through an antisense effect.[17] Indeed, an in vitro strand-exchange experiment produced a mobility shift of the **suDNP** band following the addition of sense RNA complementary to the 20-mer AS DNA of the **suDNP** (Figure 3b, lane 4). Interestingly, TEM investigation of the **suDNP** and S RNA mixture revealed a transition of the toroid into entangled fibers, which suggests the formation of amyloid-like cross-β structures. DLS analysis also confirmed the formation of larger objects after S RNA binding (Supporting Information, Figure S10). The binding of S RNA and the subsequent AS DNA/S RNA duplex formation would suppress the reciprocal (orthogonal) self-assembly and increase the volume fraction of the hydrophilic segment (that is, the oligonucleotide segment, which would be switched from the double-stranded DNA to the DNA/RNA duplex). The consequence would be the formation of a β-sheet-mediated 1D fiber, which can be further entangled to form higher-order structures. Occasionally, giant toroids of approximately 300 nm could be observed. Although determining the exact structure of these giant toroids would need further studies, the structure is reminiscent of the DNA toroid, a structure in which DNA is packaged at its physical limit.[18] The structural transition to entangled fibers and higher-order structures can be an advantageous factor during the interference of mRNA binding to ribosomes. The structural stability of the **suDNP** might be further controlled by adjusting the thermodynamic stability of the DNA/DNA duplex within the **suDNP** relative to that of the DNA/mRNA duplex.

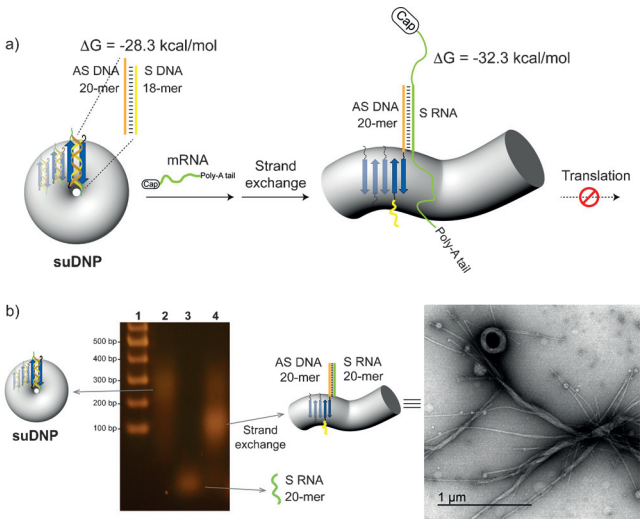

Figure 3. Supramolecular nanostructures for programmable antisense effects. a) Antisense inhibition of gene expression by the **suDNP** through DNA and RNA strand exchange. b) Strand-exchange experiment. Lane 1, DNA ladder; lane 2, suDNP; lane 3, 20-mer sense RNA (S RNA); and lane 4, **suDNP** + S RNA. Electrophoresis was performed in a 2% agarose gel after 1 d of the strand exchange reaction. A negative-stain TEM image shows the sample under the same conditions as in the lane 4. The ΔG values were calculated using nearest-neighbor models.[14]

We investigated the antisense effect of the **suDNP** in a tissue culture gene knockdown experiment. HeLa cells were first transfected with a GFP expression vector for 4 h. The cells were then washed and treated with the **suDNP** for 4 h or 8 h. As a control, single-stranded AS DNA (ssAS DNA) or AS DNA/S DNA duplex was transfected using a commercial

transfection agent, Lipofectamine 2000 (lipoplex), for 4 h or 8 h. The cells were washed and further incubated for 1 d, and changes in the GFP expression level were monitored with fluorescence-activated cell sorting (FACS; Figure 4a, and the Supporting Information, Figures S11 and S12). The results showed that the **suDNP** did exert the antisense effect and the degree of inhibition for the **suDNP** was approximately 50% that of the lipoplex. Considering the high transfection efficiency of Lipofectamine 2000, the **suDNP** had a substantial antisense effect. We then synthesized a **suDNP** in which the RGD sequence had been replaced with RAD. Such a mutation has been reported to weaken the binding affinity to the integrin receptor.[19] A gene knockdown experiment showed a decreased level of GFP expression with the RAD-based **suDNP**, which supports the enhanced uptake of RGD-based **suDNP** through RGD-integrin interactions (Supporting Information, Figure S13). The cytotoxicity of the material was measured under the same treatment conditions as for the inhibition experiment (Figure 4b). Interestingly, the **suDNP** did not exhibit notable cytotoxicity at the concentration range tested. In contrast, significant cytotoxicity was observed for the lipoplex.

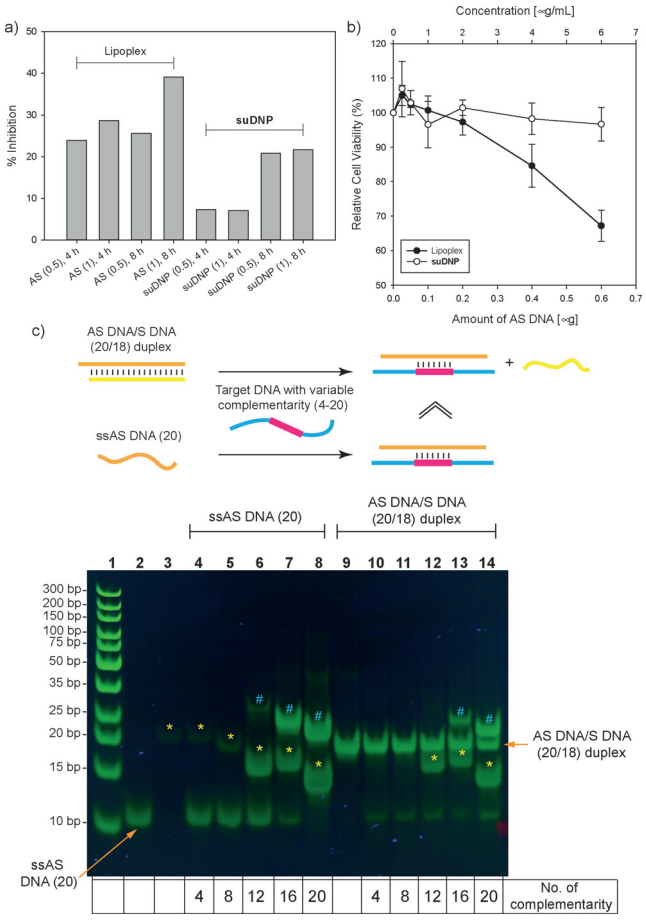

Figure 4. Antisense effect of **suDNP**. a) Inhibition of GFP expression levels. The numbers in parentheses indicate the amount of AS DNA used in μg. The experiment was replicated in the laboratory five times. b) MTT assay for cytotoxicity measurement. Mean ± s.d. ($n = 3$). c) Mismatch recognition experiment. 24-mer single-stranded target DNAs with complementary sequences of different lengths (⋆). AS DNA/target DNA duplex (#). Electrophoresis was performed in 15% polyacrylamide. Lane 1, marker; lane 2, ssAS DNA; lane 3, target DNA with 4-complementarity; lane 9, AS DNA/S DNA duplex; mixtures of ssAS DNA (lanes 4–8) and AS DNA/S DNA duplex (lanes 10–14) with target DNAs containing variable degrees of complementarity (shown below the image of the gel).

Although many factors are likely responsible for the observed difference in cytotoxicity between the **suDNP** and the lipoplex, we would like to discuss the benefits of programming the ΔG of hybridization in the duplex platform. Utilizing duplex instead of ssAS DNA can be advantageous by decreasing nonspecific binding. In contrast to ssAS DNA, which is fully exposed to the external environment, a programmed duplex is less likely to bind to other single-stranded oligonucleotides unless the final state of the strand-exchange reaction has a lower free energy. Experimentally, we demonstrated this notion using a model mismatch-recognition system in which target single-stranded DNAs with different numbers of complementary bases were incubated with ssAS DNA (20-mer) or AS DNA/S DNA (20-mer/18-mer) duplex (Figure 4c and the Supporting Information, Figure S14). Increasing the degree of complementarity tended to promote more efficient target DNA recognition in both groups; however, the formation of AS DNA/target DNA duplexes occurred with lower degrees of complementarity for the ssAS DNA than for the AS DNA/S DNA duplex. Thus, the duplex with programmable stability exhibited higher specificity than the simple ssAS DNA. The result demonstrates that the consideration of the thermodynamic stability during the design of the **suDNP** can be a strategy for decreasing the side effects of an antisense system.

In this study, we have demonstrated the assembly of well-defined and programmable supramolecular peptide/DNA complexes from PDCs. The covalent linkage between the two orthogonal building blocks likely constrains the structural space of the assembled states, thus reducing the probability of nonspecific aggregate formation. The gene regulation function of the **suDNP** can be fine-tuned by adjusting the stability of the DNA duplex segment. We envision that further supramolecular controls from this prototype will enable the development of artificial DNPs with more sophisticated structures and functions.

Acknowledgements

TEM data acquisition and image processing were performed at the Division of Electron Microscopy Research, Korea Basic Science Institute. This work was supported by grants from the National Research Foundation (NRF) of Korea (2014R1A2A1A11050359, 2014M3A7B4051594) and Yonsei University Future-leading Research Initiative.

Keywords: deoxyribonucleoproteins · DNA structures · peptide–DNA conjugates · peptides · self-assembly

How to cite: *Angew. Chem. Int. Ed.* **2016**, *55*, 12003–12007
Angew. Chem. **2016**, *128*, 12182–12186

[1] a) D. E. Discher, A. Eisenberg, *Science* **2002**, *297*, 967 – 973; b) M. Lee, B. K. Cho, W. C. Zin, *Chem. Rev.* **2001**, *101*, 3869 – 3892; c) E. Mattia, S. Otto, *Nat. Nanotechnol.* **2015**, *10*, 111 – 119.
[2] a) R. V. Ulijn, D. N. Woolfson, *Chem. Soc. Rev.* **2010**, *39*, 3349 – 3350; b) H. M. König, A. F. Kilbinger, *Angew. Chem. Int. Ed.* **2007**, *46*, 8334 – 8340; *Angew. Chem.* **2007**, *119*, 8484 – 8490; c) Y. B. Lim, K. S. Moon, M. Lee, *Chem. Soc. Rev.* **2009**, *38*, 925 – 934; d) E. Gazit, *Chem. Soc. Rev.* **2007**, *36*, 1263 – 1269; e) M. R. Ghadiri, J. R. Granja, R. A. Milligan, D. E. McRee, N. Khazanovich, *Nature* **1993**, *366*, 324 – 327.
[3] a) S. M. Douglas, H. Dietz, T. Liedl, B. Hogberg, F. Graf, W. M. Shih, *Nature* **2009**, *459*, 414 – 418; b) Y. Ke, L. L. Ong, W. M. Shih, P. Yin, *Science* **2012**, *338*, 1177 – 1183; c) T. Gerling, K. F. Wagenbauer, A. M. Neuner, H. Dietz, *Science* **2015**, *347*, 1446 – 1452.
[4] a) D. N. Nguyen, J. J. Green, J. M. Chan, R. Langer, D. G. Anderson, *Adv. Mater.* **2009**, *21*, 847 – 867; b) E. Mastrobattista, M. A. van der Aa, W. E. Hennink, D. J. Crommelin, *Nat. Rev. Drug Discovery* **2006**, *5*, 115 – 121.
[5] a) Y. B. Lim, E. Lee, Y. R. Yoon, M. S. Lee, M. Lee, *Angew. Chem. Int. Ed.* **2008**, *47*, 4525 – 4528; *Angew. Chem.* **2008**, *120*, 4601 – 4604; b) A. Hernandez-Garcia, D. J. Kraft, A. F. Janssen, P. H. Bomans, N. A. Sommerdijk, D. M. Thies-Weesie, M. E. Favretto, R. Brock, F. A. de Wolf, M. W. Werten, P. van der Schoot, M. C. Stuart, R. de Vries, *Nat. Nanotechnol.* **2014**, *9*, 698 – 702.
[6] a) K. Ding, F. E. Alemdaroglu, M. Borsch, R. Berger, A. Herrmann, *Angew. Chem. Int. Ed.* **2007**, *46*, 1172 – 1175; *Angew. Chem.* **2007**, *119*, 1191 – 1194; b) F. E. Alemdaroglu, N. C. Alemdaroglu, P. Langguth, A. Herrmann, *Adv. Mater.* **2008**, *20*, 899 – 902.
[7] K. Luger, A. W. Mader, R. K. Richmond, D. F. Sargent, T. J. Richmond, *Nature* **1997**, *389*, 251 – 260.
[8] a) C. H. Tung, S. Stein, *Bioconjugate Chem.* **2000**, *11*, 605 – 618; b) M. K. Lee, Y. B. Lim, *Bioorg. Med. Chem.* **2014**, *22*, 4204 – 4209; c) S. Peyrottes, B. Mestre, F. Burlina, M. J. Gait, *Tetrahedron* **1998**, *54*, 12513 – 12522; d) N. Venkatesan, B. H. Kim, *Chem. Rev.* **2006**, *106*, 3712 – 3761.
[9] a) N. Hirota, K. Mizuno, Y. Goto, *Protein Sci.* **1997**, *6*, 416 – 421; b) R. Xue, S. Wang, C. Wang, T. Zhu, F. Li, H. Sun, *Biopolymers* **2006**, *84*, 329 – 339.
[10] J. Kypr, I. Kejnovska, D. Renciuk, M. Vorlickova, *Nucleic Acids Res.* **2009**, *37*, 1713 – 1725.
[11] E. Cerf, R. Sarroukh, S. Tamamizu-Kato, L. Breydo, S. Derclaye, Y. F. Dufrene, V. Narayanaswami, E. Goormaghtigh, J. M. Ruysschaert, V. Raussens, *Biochem. J.* **2009**, *421*, 415 – 423.
[12] a) W. Park, C. R. Midgett, D. R. Madden, G. S. Chirikjian, *Int. J. Rob. Res.* **2011**, *30*, 730 – 754; b) E. J. Boekema, M. Folea, R. Kouril, *Photosynth. Res.* **2009**, *102*, 189 – 196.
[13] a) B. S. Li, K. K. L. Cheuk, F. Salhi, J. W. Y. Lam, J. A. K. Cha, X. D. Xiao, C. L. Bai, B. Z. Tang, *Nano Lett.* **2001**, *1*, 323 – 328; b) W. J. Jeong, S. Han, H. Park, K. S. Jin, Y. B. Lim, *Biomacromolecules* **2014**, *15*, 2138 – 2145.
[14] a) N. Sugimoto, S. Nakano, M. Katoh, A. Matsumura, H. Nakamuta, T. Ohmichi, M. Yoneyama, M. Sasaki, *Biochemistry* **1995**, *34*, 11211 – 11216; b) N. Sugimoto, S. Nakano, M. Yoneyama, K. Honda, *Nucleic Acids Res.* **1996**, *24*, 4501 – 4505.
[15] a) S. Peng, F. Ding, B. Urbanc, S. V. Buldyrev, L. Cruz, H. E. Stanley, N. V. Dokholyan, *Phys. Rev. E* **2004**, *69*, 041908; b) S. Han, D. Kim, S. H. Han, N. H. Kim, S. H. Kim, Y. B. Lim, *J. Am. Chem. Soc.* **2012**, *134*, 16047 – 16053.
[16] T. F. De Greef, M. M. Smulders, M. Wolffs, A. P. Schenning, R. P. Sijbesma, E. W. Meijer, *Chem. Rev.* **2009**, *109*, 5687 – 5754.
[17] N. Dias, C. A. Stein, *Mol. Cancer Ther.* **2002**, *1*, 347 – 355.
[18] L. R. Brewer, *Integr. Biol.* **2011**, *3*, 540 – 547.
[19] M. G. Overstreet, A. Gaylo, B. R. Angermann, A. Hughson, Y. M. Hyun, K. Lambert, M. Acharya, A. C. Billroth-Maclurg, A. F. Rosenberg, D. J. Topham, H. Yagita, M. Kim, A. Lacy-Hulbert, M. Meier-Schellersheim, D. J. Fowell, *Nat. Immunol.* **2013**, *14*, 949 – 958.

Received: June 13, 2016
Revised: July 22, 2016
Published online: August 24, 2016

